Cellulose nanocrystals as promising nano-devices in the biomedical field

Cite as: AIP Conference Proceedings **1990**, 020019 (2018); https://doi.org/10.1063/1.5047773
Published Online: 23 July 2018

Barbara La Ferla, Luca Zoia, Paolo Bigini, and Patrizia Di Gennaro

Cellulose Nanocrystals as Promising Nano-Devices in the Biomedical Field

Barbara La Ferla,[1,a] Luca Zoia,[2] Paolo Bigini,[3] Patrizia Di Gennaro[1]

[1]*Department of Biotechnology and Biosciences, University of Milano-Bicocca, Piazza della Scienza 2, 20126 Milan, Italy*
[2]*Department of Earth and Environmental Science, University of Milano-Bicocca, Piazza della Scienza 1, 20126 Milan, Italy*
[3]*IRCCS-Istituto di Ricerche Farmacologiche "Mario Negri", via La Masa 19, 20156 Milan, Italy*

[a)]Corresponding author: barbara.laferla@unimib.it

Abstract. We present our application of cellulose nanocrystals (CNCs) in the biomedical field. With the aim of identifying novel nanoparticles for drug targeting, we fluorescently labelled the CNCs and carried out a biodistribution study in vivo. Results evidence that CNCs have a peculiar and transient tropism to the limb bones that is likely related to the interaction with the Ca^{2+} deposits in the bone matrix. We also analyzed and demonstrated the ability of CNCs to inhibit bacterial adhesion to host tissue. All these findings, taken together, make these nanoparticles very promising candidate for a potential development of nano-devices toward bone diseases, as well as new antibacterial agents.

INTRODUCTION

Cellulose-Nano-Crystals (CNCs), thanks to their physico-chemical properties, low production cost and abundance, are a potential candidate material for the development of new emerging nano-tools in the biomedical field. They can be easily obtained through an acidic hydrolysis from many cellulose source including agricultural residues [1-7]. These NPs present a rod-shape morphology that has been reported to possess higher specificity versus endothelial targets compared to their spherical counterparts [8] , thus suggesting a potential use of elongated NPs for theranostic purposes [9], with particular application towards bone-disorders [10-12], the cure of which is extremely challenging due to the very low tropism of drugs towards this target [13]. Under the molecular point of view, these NPs are constituted by packed linear saccharide polymers, made of β(1-4) linked glucose units (Fig. 1a), and present sulphate half-ester groups on part of the surface hydroxyl groups, introduced during the hydrolytic process. These characteristics, taken together, closely resemble the structural features of glycosaminoglycans (GAGs), one of the main constituent of extracellular matrix (ECM), that seem to be crucial for the first stage microbial adhesion process to host cell surface. This process is the key step prior to bacterial colonization and infection, as it avoids bacterial sweeping by the circulating fluids [14-28]. Therefore, the inhibition of bacterial adhesion through the use of GAGs-analogues material, like CNCs, may constitute a novel antibacterial strategy.

In this paper we carried out a series of experimental evaluations in order to investigate the potential use of CNCs in the biomedical field, with particular focus on their drug targeting ability and antibacterial activity. First we extracted and fully characterized the CNCs under the chemical-physical point of view. Then we evaluated the eventual toxicity towards mammalian and bacterial cells. We carried out a careful evaluation of the biodistribution, accumulation and clearance in filter organs of CNCs in mice. To follow the fate of CNCs in living animals at

NANOINNOVATION 2017
AIP Conf. Proc. 1990, 020019-1–020019-8; https://doi.org/10.1063/1.5047773
Published by AIP Publishing. 978-0-7354-1706-9/$30.00

different time points after single administration [29] a fluorescent dye detectable by in vivo Optical Imaging was covalently linked to the crystals.

Finally, to investigate the ability of CNCs to adhere to bacterial cells and therefore to inhibit the bacterial adhesion to host cells, we used *E. coli* as bacterial model, and employed HT29 colon cancer cell line.

EXPERIMENTAL SECTION

Materials

Whatman Cellulose filter paper was purchased from Sigma Aldrich. Alexa Fluor® 633 hydrazide, bis(triethylammonium) salt was purchased from Life technologies. Dialysis tubes in Cellulose membrane with a molecular weight cut off of 12,000 Dalton were purchased from Sigma Aldrich. Dulbecco's Modified Eagle's Medium - high glucose (DMEM 4500 mg/L glucose, with/without L-glutamine, and with/without sodium bicarbonate, without sodium pyruvate, liquid, sterile-filtered, suitable for cell culture, Sigma Aldrich), Fetal Bovine Serum (FBS, USA origin, sterile-filtered, suitable for cell culture, Sigma Aldrich), Phosphate Buffered Saline (PBS, 10 × concentrate, with/without Ca^{2+}/Mg^{2+}, BioPerformance Certified, suitable for cell culture, Sigma Aldrich), Hoechst-33258 (Hoechst-33258, Pentahydrate (bis-Benzimide) - 10 mg/mL Solution in Water, Molecular ProbesTM), Fluormount (fluormount mounting medium, 25 ml, Bio-Optica), Ketamine hydrochloride solution (1.0 mg/mL in methanol, Sigma Aldrich).

Preparation of CNCs and Alexa Fluor® 633 labelled CNCs

CNCs were extracted from Whatman filter paper by acid hydrolysis in 64% H_2SO_4 for 1 h at 55ºC at acid/Cellulose ratio of 10 w/w. After acidic treatment, the content of the flask was poured into ten-fold volume of cold water and stirred. Cellulose sediment was purified by repeated cycles of centrifugation at the acceleration of 3200 g for 15 minutes and the re-suspension of the solid component with distilled water was carried out by ultrasonic mixing for 5 minutes. After obtaining a turbid supernatant, the suspension was dialyzed against distilled and ultrapure Milli-Q® water for 1 week until pH of 6 was reached. The obtained CNCs have been functionalized according to a modification of the procedure developed by Huang et al. [30]. To a suspension of CNCs (0.5%, 25 ml), 1 mg of Alexa Fluor® 633hydrazide, bis(triethylammonium) salt and 200 µL of acetic acid were added. The mixture was left to react at room temperature in the dark. After 24 h the mixture was dialyzed against distilled water for 1 week in order to remove the acetic acid and the unreacted fluorophore. Before all the *in vitro*, *in vivo*, *ex vivo* experiments, CNCs were separated from any precipitate by centrifugation at 6000 rpm for 5 minutes and then sterilized under UV light for at least 1 h.

Characterization of CNCs was performed by UV-Vis spectroscopy, AFM analysis and DLS measurements. The UV-Vis absorption spectra were collected with a UV-Vis spectrophotometer Evolution 300 (Thermo Scientific). We also performed a conductimetric titration [31]. For AFM analysis, 500 µL of sample of the CNSs were diluted with 950 µL of distilled water, and 50 µL were immediately added onto freshly cleaved mica at room temperature for five minutes: samples were washed and dried under gentle nitrogen flow. AFM analyses were carried out on a Multimode AFM with a Nanoscope V system (Veeco/Digital Instruments, Mannheim, Germany) operating in tapping mode, using standard antimony(n) doped silicon probes (T: 3.5 – 4.5 µm, L: 115 – 135 µm, K: 20 – 80 N/m) (Bruker Corporation, Billerica, Massachusetts, USA) with a scan rate in the 0.5 – 1.2 Hz range, proportionally to the area scanned and the images were acquired in Height and Amplitude Error. AFM images were analyzed by Scanning Probe Image Processor (SPIP-version-5.1.6, release 13 April 2011) data analysis package. To exclude the interference of possible artefacts, extra control samples, such as freshly cleaved mica and freshly cleaved mica soaked with buffer, were also used. All the topographic patterns and SPIP characterization described were repeated by additional measurements on a minimum of five different well separated areas.

Dynamic Light Scattering (DLS) and Zeta-potential measurements were performed, using a Zeta Sizer Nano 3600 (Malvern), operating laser (λ = 632.8 nm), using a backscattering angle of 173°. The zeta potential was determined with the same instrument and data were processed by Zetasizer Software 7.03. The samples were prepared by dilution of initial particles stock solution 7g/L in Milli-Q® water obtaining the final concentration of 140 mg/L. Measurements were carried out at 25°C, using a disposable cuvette with 10 mm optical path length. Three replicate measurements per sample were performed to establish measurements repeatability.

Cellular Cytotoxicity

HeLa cells (ATCC CCL-2; from human cervix adenocarcinoma) were selected as cellular line model in order to evaluate CNCs cytotoxicity; HeLa cells (15,000/well) were seeded in quadruplicate in 96-well plate and treated with increasing concentrations of CNCs (14 µg/mL, 37 µg/mL, 70 µg/mL, 140 µg/mL), for 6 h, 24 h, and 48 h. The medium without NPs was added as a control. At the end of the treatment cell proliferation was determined by MTS assay using CellTiter 96Aqueous cell proliferation assay kit (Promega). The optical density of each well was measurement by using Infinite ® 200 microplate reader (Tecan) at 490 nm. The number of living cells were compared in presence and absence of CNCs.

Bacterial survival and growth: the minimum inhibitory concentration of the CNCs against *E. coli* ATCC 25922 was determined using a dilution method and by subculturing the test dilutions on TSA agar plates after incubation for 24h. The concentration at which there was no growth on agar plates was taken as minimum bactericidal concentration. The determinations were performed in triplicate and the means of three independent experiments were calculated. Growth experiments were conducted without or with 1% of CNCs in a solution containing 1 x 106 cells of *E. coli* ATCC 25922, incubated for 24h. After incubation the microbial suspensions were plated on LB agar plates. Counts were carried out at 48h and 96h.

In vivo analysis

For *in vivo* analyses, 3-month-old female NFR mice were used. Animals were bred and maintained under specific pathogen free condition in the Institute's Animal Care Facilities; they received food and water *ad libitum* and were regularly checked by a certified veterinarian who is responsible for animal welfare supervision and experimental protocol revision. Procedures involving animals and their care were conducted in conformity with the institutional guidelines at the IRCCS-Institute for Pharmacological Research “Mario Negri” in compliance with national (Decreto Legge nr 116/92, Gazzetta Ufficiale, supplement 40, February 18, 1992; Circolare nr 8, Gazzetta Ufficiale, July 14, 1994) and international laws and policies (EEC Council Directive 86/609, OJL 358, 1, Dec. 12, 1987; Guide for the Care and Use of Laboratory Animals, US National Research Council, 8th edition, 2011). This project of research has been reviewed by IRCCS-IRFMN Animal Care and Use Committee (IACUC) and then approved by the Italian “Istituto Superiore di Sanità” (code: 17/01 D Appl 3). A suspension of CNCs NP, in 120 µL of sterile PBS at a concentration of 35 µg/mL were injected in the tail vein. Vehicle treated animals received the same volume of sterile PBS without NPs. For *in vivo* studies Optical Imaging was conducted on animals before and at 1h, 24 h and 7 days after CNCs injection using Explore Optix System (ART Advanced Research Technologies, Montreal, Canada), as already described by our group [32]. Selected region of interest (ROI) scan (ventral whole body, tail and hind leg) was performed with a step size of 2 mm. At the end of each scanning, animals were placed in their cage, no sufferance or stress was recorded during the whole duration of the experiments.

Fluorescent microscopy

Agarized glass slides were used to immobilize *E. coli* in the presence and absence of CNCs at the concentration of 0.1 %. The CNCs were stained with Alexa Fluor 633 (Ex/Em of the conjugate: 624/643 nm); and bacteria were stained with SYBR® Safe DNA Gel Stain (Ex/Em of the conjugate: 497/520 nm). The stained CNCs and stained bacteria were analysed with a Fluo View FV100 (Olympus) Fluorescence Microscopy.

Bacteria adhesion assay

HT29 (ATCC® HTB-38™) colon cancer cell line was grown in DMEM medium supplemented with heat-inactivated 10% FBS, 2 mM L-glutamine, and maintained at 37°C in a humidified 5% CO_2 incubator. During routine culture we also used 100 U/mL penicillin and 100 µg/mL streptomycin. The cells were grown in 75 cm^2 flasks and subcultured every time they reach confluence. All the reagents for cell culture were supplied by Lonza (Lonza Group, Basel, Switzerland).

In order to perform bacterial adhesion experiments, the cells were incubated with 0.05% trypsin-EDTA for 5 min and then fresh warm medium supplemented with 10% FBS and 2 mM L-glutamine but containing no antibiotics was added. The cell suspension was homogenized by repeated up-and-down pipetting and centrifuged at 1200 rpm for 10

min. The pellet was resuspended in the same medium and the cells were seeded at a density of 2.5×10^4 cells/well into a 96-well plate and incubated for 24 h in a cell culture incubator.

Bacterial adhesion assay was performed to evaluate the effect of cellulose nanoparticles (CNCs) on adherence of *E. coli* ATCC 25922 on a monolayer of human epithelial intestinal HT29 cells. The monolayer of HT29 cells in DMEM medium was prepared in a 96 multi-well plate as described above and left in incubation for 24h at 37°C. Then the microbial suspension containing 1 x 106 cells of *E. coli* pre-incubated with CNCs at two different times of incubation 2h and 24h was added on the monolayer in PBS. A fresh culture of *E. coli* on LB broth was prepared and when the culture reached the O.D. of 0.7 at 600 nm, cells (0.1 mL of the culture) were collected by centrifugation at 12000 rpm for 2 min and pre-incubated in 1 mL of nanoparticles suspension at the concentration of 0.1%. Then the suspension of *E. coli* pre-incubated with CNCs was centrifuged at 12000 rpm for 2 min, to remove CNCs not adhering to bacterial cells, and re-suspended in 1 mL of PBS. The supernatant of the prepared 96 multi-well plate containing the monolayer was removed and 100 µL of *E. coli* pre-incubated with CNCs suspension was added. The 96 multi-well plate containing monolayer bacteria and CNCs were incubated under a 5% CO_2 atmosphere for 3 h at 37°C. After incubation the supernatant containing bacteria in suspension was removed and a washing procedure with PBS was performed. Then 100 µL of 1% TritonX100 solution with incubation for 10 min at room temperature was used for the detachment of the attached cells to HT29 from the surface. At this point we determined the number of bacteria by counts on plates. A serial dilution of microbial suspension was performed and plated on TSA agar medium; after over-night incubation at 37°C the CFU/mL of bacteria were determined. Planktonic and adhered cells were quantified using the CFU/mL counts and expressed in percentage.

Data calculation and statistical analysis

All data were expressed as mean ± S.D. One-way analysis of variance (ANOVA), followed by Bonferroni's post-test analysis, was used. All statistical analyses were done using the GraphPad Prism version 6.00 for Windows (Graph-Pad Software, San Diego, CA, USA)

RESULTS AND DISCUSSION

CNCs were extracted from Whatman#1 filter paper by acid hydrolysis in 64% H_2SO_4 and characterized by UV-Vis spectroscopy, AFM, TEM analysis (Fig. 1b) and DLS measurements. Among the different characteristics, particular attention was devoted to the surface of the CNCs. This is characterized by the presence of different hydroxyl groups of cellulose and negatively charged sulphate half-ester groups introduced during the extraction. We performed DLS measurements and we found a ζ-potential of -39.0 ±1.0 mV and a dimension of 92.4 ± 1.8 nm in agreement with the literature [33]. The strong acid sulphate half-ester groups produce the negative ζ-potential and consequently confer the colloidal stability to the aqueous CNCs suspension. We performed a conductometric tritation [34] to quantify the sulphate half ester we found a value of 0.17 mmol/g for R-OSO_3H. Assuming a model of CNC 10 nm wide and 200 nm long (from TEM and AFM analyses) and considering the length of a glucan chain approximately 0.52 nm, the CNC model is roughly 20×20×385 AGU (anhydroglucan unit), with a total of 154000 AGU per nanoparticle. However the AGU present on the surface are 20×4×385, with a total of 30800 AGU. Due to the fact that the total primary hydroxyl groups of the glucan unit are 6.2 mmol/g (1/162 mol/g), in order to calculate the amount of primary alcohols on the CNC surface we must divided 6.2 by (154000/30800) and the result again by 2 because half of the primary alcohols are involved in internal hydrogen bond. The result is around 0.62 mmol/g, indicating that around 30% of the primary hydroxyl groups exposed on the surface of a CNC has been converted during the extraction process in sulphate half-ester groups (0.62 vs 0.17 mmol/g), roughly 8500 R-OSO_3^- for a single CNC model nanoparticle. We also synthesized the fluorescently labelled CNCs to perform both the in vivo and the bacterial adhesion study. The Alexa Fluor®633 hydrazidebis(triethylammonium) was covalently linked to the reducing end of CNCs, the fluorofore content on CNCs was determined by UV/Vis spectroscopy. Figure 1b (lower panel) shows the UV/Vis absorption spectra in pure water (pH 7.0) of Alexa Fluor®633 labeled CNCs and of unlabeled ones. The spectrum of the Alexa Fluor®633 labeled CNCs (black line) showed maxima peaks at 560 and 630 nm, while unlabeled CNCs (dot line) did not show any specific absorption peak. The DLS measurements was conducted before and after labelling, and we found a ζ-potential of -39.0 ±1.0 mV and a dimension of 92.4 ± 1.8 nm (before functionalization) and a ζ-potential of -40.6 ±1.3 mV and a dimension of 105.0 ± 6.1 after functionalization, in agreement with the literature [33]

Before performing any further study, we evaluated the eventual toxicity of CNCs towards both mammalian and bacterial cells. HeLa cells (ATCC CCL-2; from human cervix adenocarcinoma) were selected as cellular model and an MTS Assay was carried out at different NPs concentrations ranging from 14 to 1400 μg/mL, and no toxic effect was observed (Fig. 2a).

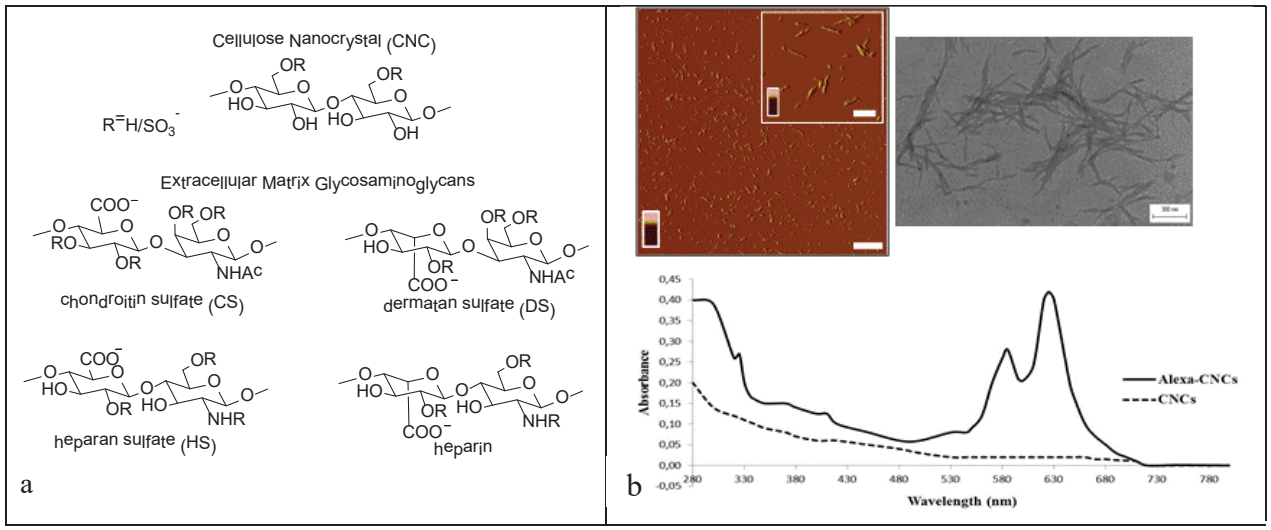

Figure 1: **a)** Chemical structures repeating disaccharidic units of GAGs and of cellulose nanocrystal. **b) upper panel (left)** Representative tapping mode of AFM images as determined by height data of CNCs (Z range: −5/+20 nm). Scale bar, 2 μm; inset, 100 nm; **(right)** TEM analysis of extracted CNCs. **Lower panel** UV-Vis spectra of CNCs before and after modification with Alexa Fluor® 633.

Bacterial survival and growth were carried out using *E. coli* ATCC 25922 in the presence of CNCs to evaluate the toxicity on bacterial cells. Growth experiments were conducted without or with 1% of CNCs in a solution containing 1 x 10^6 cells of bacterial cells. After 48 h no colony were detected in the plates containing the microbial suspension incubated with the CNCs, but in the same plates, after 96 h, the initial bacterial number was observed. The results clearly indicated that CNCs are not toxic for bacteria and their survival is not compromised at concentrations of nanoparticles used in this study. From this experiment we also observed a slowdown of *E. coli* growth in the time frame monitored (96 h) (data not shown). We hypothesize that this effect could be probably due to the adhesion of the nanocrystals on the bacteria cell membrane, that slowed down the reproduction ability of *E. coli* with respect to the bacteria not incubated with CNCs.

Once verified the lack of cytotoxicity of the CNCs on both mammalian and bacterial cells we carried out the key experiments to verify the ability of CNCs to be used as nanovectors for drug delivery and as potential antibacterial agents. For the former task analyses in living animals were carried out. A solution of 120 μL of CNCs (3.5 μg/mL) was intravenously administrated in healthy mice and the main kinetic parameters (e.g., biodistribution, bioaccumulation, clearance) were examined by a combined strategy coupling non-invasive *in vivo* imaging analysis to *ex vivo* studies. A longitudinal pattern of CNCs bio-distribution is shown in Fig. 2b.

One hour after CNCs administration a strong signal was found in the mid and cranial portions of the abdomen, likely localized at level of the liver and kidneys with a weaker fluorescence in correspondence to the pelvic region (likely related to the urinary bladder). The signal associated to the liver (right side of epigastric region) was markedly reduced 24 h after CNC administration, while it was almost absent at the last time-point (7 days). On the contrary, the signal localized in the left epigastric region, already evident 1 h after CNC administration, was also detected up until 7 days. This effect is likely due to the migration of blood cells to the spleen after CNC-uptake in the bloodstream. The rapid clearance through the excretory systems and the slower reduction from spleen is not surprising and is somehow similar to that observed for many other contrast agents. This difference is mainly related to the fact that the complete metabolism and elimination of blood cells by spleen requires a longer time in comparison to the clearance through feces and urines. At 24 h, a strong signal appeared behind the liver region, and after 7 days it was localized in the central part of the abdomen, likely overlapping the intestinal tract, and possibly suggesting a progressive accumulation of CNCs in the cecal content and therefore suggesting an efficient clearance

of the CNCs. A strong signal was found in the tail vein (the site of CNCs injection) up to 24 h after the administration. In a former study [35]also histological analyses were carried out to study the biodistribution, accumulation and clearance. Results indicates that an early excretion of CNCs occurred both via biliary and urinary routes, supporting the results of the *in vivo* imaging, where the CNC signal was detected in correspondence of the urinary bladder and intestinal tract.

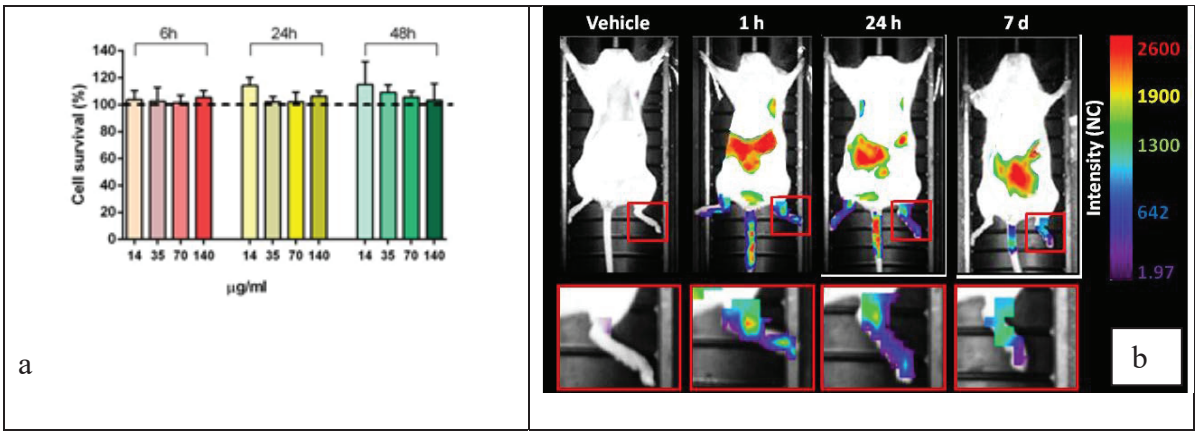

Figure 2: **a)** Histogram showing the complete absence of toxicity of CNCs in HeLa cells. Dotted line represents the average number of cells measured in vehicle-treated conditions and normalized at 100 for each time-point. **b)** Optical Imaging scans acquired before and at 1 h, 24 h and 7 d respectively after CNCs intravenous injection (a single dose of 120 µl at a concentration of 35 µg/ml). Three different regions of interest (ROI) were processed. They were the abdominal area, the tail and the distal left hind limb. In the red squares (bottom panels) a higher magnification of the distal hind limb is shown. The fluorescence intensity signal was measured as normalized photon counts (NC) and is shown as a pseudo-color scale bar. The images shown were analyzed with ART OptixOptiview software and are representative of 3 animals per group.

Very interestingly, the scanning at level of the distal portion of the left hind limb revealed the presence of CNCs-related signal; this particular localization was observed neither using polymeric nanoparticles [36] nor avidin nucleic-acid nanoassemblies [32]. We believe that the persistence of the signal at the hind limbs is due to the favorable interaction of the sulphated CNCs with the bone matrix and in particular with the positively charged calcium ion. Overall the rapid excretion by filter organs is in accordance with the high biocompatibility of this material and also strengthen the potential development as theranostic tool.

As stated in the introduction, the molecular structure of the sulphated CNCs, that seems to favor the interaction with the bone matrix, as just reported, suggested a possible analogy with the ECM components, such as heparin and heparan sulphate which are involved in the host cell bacterial adhesion process. Therefore we supposed that CNCs could adhere to bacteria cell surface, mimicking the action of ECM. To confirm this idea we performed the incubation of bacteria cells using fluorescently labelled CNCs, prepared for the previous *in vivo* biodistribution study.

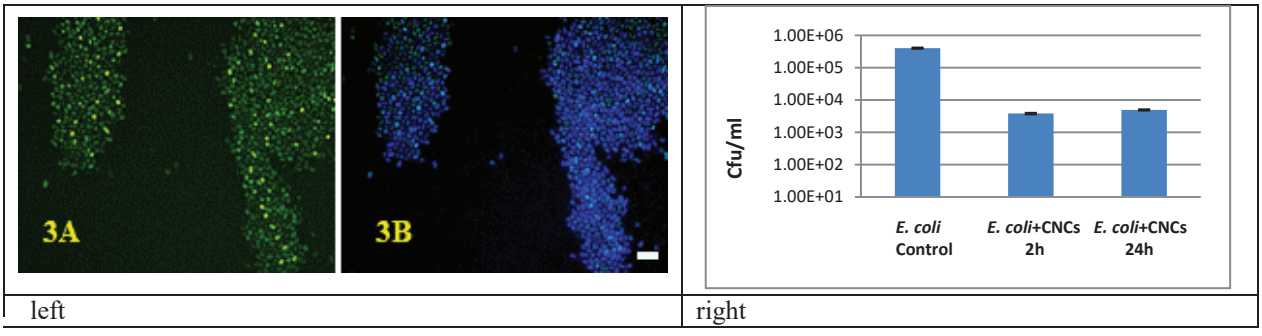

left right

Figure 3. left panel Fluorescence Microscopy: 3A Em λ 520 nm (bacteria stained with SYBR® Green); 3B merge of Em λ 520 nm and Em λ 643 nm (detecting labelled CNCs). Scale bar, 0.6 cm = 10 µm; **right panel** Inhibitory effect of nanoparticles on adherence of *E. coli* to monolayer of HT29 cells. The determinations were performed in triplicate and the means of three independent experiments were calculated

Then, the Alexa Fluor® 633 labelled CNCs (0,1%) were pre-incubated with a culture of *E. coli* (1 x 10^6 cells) 2h and analyzed to fluorescence microscopy after the addition of SYBR® Green stain to evidence bacteria (Fig. 3 left panel). The superimposition of the images acquired reading at Em λ 520 nm (spotting in green live bacterial cells), and at Em λ 643 nm (evidencing the CNCs in blue) (Fig. 3B) clearly shows that CNCs are perfectly co-localized with the bacteria (Fig. 3A), therefore supporting the hypothesis that CNCs may directly adhere to bacteria.

To verify the ability of CNCs to inhibit bacterial adhesion to host cells we performed adhesion inhibition experiments using human epithelial intestinal HT29 cell line. To a monolayer of HT29 cells, a well-known human intestinal epithelial model cell line, after confluence was reached, was added a microbial suspension containing 1 x 10^6 cells of *E. coli* pre-incubated with CNCs, centrifuged, to remove CNCs not adhering to bacterial cells, and re-suspended in 1 mL of PBS. The cell adhesion experiment was performed in PBS and applying two different times of pre-incubation of the bacteria with the nanoparticles, t2h and t24h. The different bacteria suspensions were left in incubation with the cells at 37°C for 3 h. After incubation, bacteria in suspension were removed and after a washing procedure, the monolayer with the adherent bacteria was removed from the multi-well. At this point we determined the number of bacteria by counts on plates (Fig. 3 right panel). Results showed an inhibition of the adhesion of *E. coli* cells to the monolayer at least of two logs with respect to the *E. coli* cells not pre-incubated with nanoparticles.

CONCLUSIONS

The lack of toxicity associated to CNCs towards mammalian cells, along with the peculiar and transient tropism to the limb bones, and with the easy derivatization procedure that exploits the reducing end-group of the terminal glucose unit, suggest the future conjugation with drugs to be considered as potential therapeutic agent able to target bone tissue. Moreover, the ability of CNCs to inhibit *E. coli* ATCC 25922 adhesion to the intestinal HT29 cell line, not due to a bactericidal effect of the CNCs, indicates that these nanoparticles could be ideal for the prevention of the adhesion effect of potential pathogen strain on human cell lines. Thus, CNCs nanoparticles could be possibly used as a topical applicant to prevent *E. coli* or other bacterial infections.

REFERENCES

1. Y. Habibi, L. A. Lucia, O. J. Rojas, Chem Rev., **110**, 3479-500 (2010).
2. G. Siqueira, H. Abdillahi, J. Bras, A. Dufresne, Cellulose, **17**, 289-298 (2010).
3. R. M. Sheltami, I. Abdullah, I. Ahmad, A. Dufresne, H. Kargarzadeh, Carbohydrate Polymers, **88**, 772-779 (2012).
4. S. M. L. Rosa, N. Rehman, M. I. G. de Miranda, S. M. B. Nachtigall, C. L. D. Bica, Carbohydrate Polymers **87**, 1131-1138 (2012).
5. N. Johar, I. Ahmad, A. Dufresne, Industrial Crop and Products, **37**, 93-99 (2012).
6. P. Lu, Y. L. Hsieh, Carbohydrate Polymers, **87**, 564-573 (2012).
7. I. Filpponen, D. S. Argyropoulos, Biomacromolecules, **11**, 1060-1066 (2010).
8. P. Kolhar, A. C. Anselmo, V. Gupta, K. Pant, B. Prabhakarpandian, E. Ruoslahti, S. Mitragotri, PNAS, **110**, 10753-10758 (2013).
9. A. Pistone, G. Grassi, S. Galvano, Curr. Med. Chem., **20**, 1333-1354 (2013).
10. J. C. Kraft, J. P. Freeling, Z. Wang, R. J. Ho, J. Pharm. Sci., **103**, 29-52 (2014). Review.
11. M. J. Ernsting, M. Murakami, A. Roy, S. D. Li, J. Control. Release., **172**, 782-794 (2013).
12. F. Alexis, E. Pridgen, L. K. Molnar, O. C. Farokhzad, Mol. Pharm., **5**, 505-15 (2008**)**.
13. P. Decuzzi, R. Pasqualini, W. Arap, M. Ferrari, Pharma Res., **26**, 235-43 (2009).
14. K. S. Rostand, J. D. Esko, Infect. Immun., **65**, 1 (1997).
15. T. Wadström, A. Ljungh, J. Med. Microbiol., **48**, 223 (1999).
16. C. Alvarez-Domínguez, J.-A. Vázquez-Boland, E. Carrasco-Marín, P. López-Mato, F. Leyva-Cobián, Infect. Immun., **65**, 78 (1997).
17. F. P. de Vries, R. Cole, J. Dankert, M. Frosch, J. P. van Putten, Mol. Microbiol., **27**, 1203 (1998).
18. T. Chen, R. J. Belland, J. Wilson, J. Swanson, J. Exp. Med., **182**, 511 (1995).
19. C. C. Grant, M. P. Bos, R. J. Belland, Mol. Microbiol., **32**, 233 (1999).
20. V. Dupres, C. Verbelen, D. Raze, F. Lafont, Y. F. Dufrêne, Chemphyschem, **10**, 1672 (2009).

21. I. G. Sava, F. Zhang, I. Toma, C. Theilacker B. Li, T. F. Baumert, O. Holst, R. J. Linhardt, J. Huebner, J. Biol. Chem., **284**, 18194 (2009).
22. K. Asano, I. Kakizaki, A. Nakane, Biochimie, **94**, 1291 (2012).
23. M. Henry-Stanley, D. J. Hess, S. L. Erlandsen, C. L. Wells, SHOCK, **6**, 571 (2005).
24. E. I. Castañeda-Roldan, F. Avelino-Flores, M. Dall'Agnol, E. Freer, L. Cedillo, J. Dornand, J. A. Girón, Cel. Microbiol., **6**, 435 (2004).
25. J. M. Fleckenstein, J. T. Holland, D. L. Hasty, Infect. Immun., **70**, 1530 (2002).
26. F. N. Wuppermann, J. H. Hegemann, C. A. Jantos, J. Infect. Dis., **184**, 181 (2001).
27. L. Gu, H. Wang, Y.-L. Gou, K. Zen, Biochem. Biophys. Res. Commun., **369**, 1061 (2008).
28. E. L. G. M. Tonnaer, T. G. Hafmans, T. H. Van Kuppevelt, E. A. M. Sanders, P. E. Verweij, J. H. A. J. Curfs, Microbs Inf., **8**, 316 (2006).
29. T. Tenuta, M. P. Monopoli, J. A. Kim, A. Salvati, K. A. Dawson, P. Sandin, I. Lynch, PLoS One. **6**(10), e25556 (2011).
30. J. L. Huang, C. J. Li, D. G. Gray, ACS SustainableChem. Eng. **1**, 1160-1164 (2013).
31. G. D'Orazio, L. Munizza, J. Zampolli, M. Forcella, L. Zoia, P. Fusi, P. Di Gennaro, B. La Ferla, J. Material Chem. B., **5**, 7018-7020 (2017).
32. P. Bigini, S. Previdi, E. Casarin, D. Silvestri, M. B.Violatto, S. Facchin, L. Sitia, A. Rosato, G. Zuccolotto, N. Realdon, F. Fiordaliso, M. Salmona, M. Morpurgo, ACS Nano, **8**,175-87 (2014).
33. M. Hasani, E. D. Cranston, G. Westman, D. G. Gray, Soft Matter, **4**, 2238 (2008).
34. F. Jiang, A.R. Esker, M. Roman, Langmuir, **26**(23), 17919 (2010).
35. L. Colombo, L. Zoia, M. B. Violatto, S. Previdi, L. Talamini, L. Sitia, F. Nicotra, M. Orlandi, M. Salmona, P. Bigini, B. La Ferla. Biomacromolecules, **16**, 2862 (2015).
36. L. Sitia, K. Paolella, M. Romano, M. B. Violatto, R. Ferrari, S. Fumagalli, L. Colombo, E. Bello, M.G. De Simoni, M. D'Incalci, M. Morbidelli, E. Erba, M. Salmona, D. Moscatelli, P. Bigini, J. Nanopart. Res. **16**, 2481 (2014).